Dalton Transactions

Catalytic Dioxygenation of Flavonol by MII–Complexes (M = Mn, Fe, Co, Ni, Cu and Zn)----Mimicking the MII-Substituted Quercetin 2,3-Dioxygenase

Journal:	*Dalton Transactions*
Manuscript ID:	DT-ART-05-2015-001760.R1
Article Type:	Paper
Date Submitted by the Author:	20-Jun-2015
Complete List of Authors:	Sun, Ying-Ji; Dalian University of Technology, School of Chemistry Huang, Qian-Qian; Xinxiang Medical University, Department of Chemistry Li, Pei; Dalian University of Technology, School of Chemistry Zhang, Jian-Jun; Dalian University of Technology, School of Chemistry

Dalton Transactions

Cite this: DOI: 10.1039/c0xx00000x

www.rsc.org/xxxxxx

PAPER

Catalytic Dioxygenation of Flavonol by M^{II}–Complexes (M = Mn, Fe, Co, Ni, Cu and Zn)----Mimicking the M^{II}-Substituted Quercetin 2,3-Dioxygenase

Ying-Ji Sun,* Qian-Qian Huang, Pei Li and Jian-Jun Zhang

Received (in XXX, XXX) Xth XXXXXXXXX 200X, Accepted Xth XXXXXXXXX 200X
DOI: 10.1039/b000000x

In order to get insights into the metal ion effects and the carboxylate effects on the enzymatic activity, a series of the carboxylate ligand supported transition metal complexes [M^{II}L(OAc)] (M = Mn (**1**), Fe (**2**), Co (**3**), Ni (**4**), Cu (**5**) and Zn (**6**); **LH** = 2-{[bis(pyridine-2-ylmethyl)amino]methyl}-4-methoxy benzoic acid) were synthesized and characterized as structural and functional models for the active site of various M^{II}-substituted resting quercetin 2,3-dioxygenase (2,3-QD). Their structures, spectroscopic features, redox properties, as well as the catalytic reactivity toward substrate flavonol and O_2 have been investigated in detail. The model complexes show higher enzymatic reactivity in the catalytic dioxygenation (oxidative ring opening) of substrate flavonol at lower temperature (55 − 100 °C), presumably caused by the carboxylate group in the supporting model ligand, which could lower the redox potential of the bound substrate flavonolate by electron donation. The catalytic reactivity of [M^{II}L(OAc)] exhibits notable differences and it is in a metal ion dependent order of Co (**3**) > Ni (**4**) > Zn (**6**) > Fe (**2**) > Mn (**1**) > Cu (**5**). The differences in the reactivity among them could be ascribed to the redox potential of the bound substrate flavonolate, which was drastically influenced by the metal ion via tuning the electron density of flavonolate, providing important insights into the metal ion effects and the carboxylate effects on the enzymatic activity of various M^{II}-substituted 2,3-QD. Our model complexes [M^{II}L(OAc)] are the first example of a series of structural and functional models of various M^{II}-substituted resting 2,3-QD.

Introduction

Flavonoids are polyphenolic pigments widely spread in higher plants and some fungi,[1] which are of broad interest for their antioxidant, antiradical, antimicrobial and other properties.[2–5] Degradation of dead plants results in the deposition of quercetin in soil where bacteria and fungi can activate molecular oxygen to decompose it in an oxygenative *O*-heterocyclic ring-opening reaction with concomitant release of CO by quercetin 2,3-dioxygenase (2,3-QD) (Scheme 1). The fungal Cu(II)-containing 2,3-QD have been isolated from *Aspergillus japonicus*,[6] *Aspergillus flavus*,[7] and *Aspergillus niger* DSM 821.[8] The mononuclear Cu^{II} active site from *Aspergillus japonicus* has two distinct structures, one is coordinated by three histidine imidazoles and a water molecule in a distorted tetrahedral geometry, the other is additionally coordinated by the carboxylate group of Glu73 in a distorted trigonal-bipyramidal geometry. The bacterial Fe(II)-containing 2,3-QD from *Bacillus subtilis*[9-11] also exhibits two similar distinct structures with the corresponding Cu(II)-containing 2,3-QD, which involves a distorted square pyramidal and a trigonal-bipyramidal geometry consisting of three histidine imidazoles, a water molecule and a carboxylate group of Glu at a distance of 2.44 and 2.10 Å, respectively.[9]

Under anaerobic conditions, the substrate quercetin was deprotonated by carboxylate group of Glu73 (acts as an active site base) and coordinated to the Cu(II) ion with displacement of the water molecule to form an ES (enzyme-substrate) adduct with a distorted square pyramidal geometry,[12] additionly, Glu73 could also stabilize the bound substrate through the hydrogen bond interaction.[6,13] The site direct mutation of Glu73 results in the inactive enzyme,[6] indicating that the carboxylate group of Glu73 plays an important role in the catalytic reaction.

Scheme 1

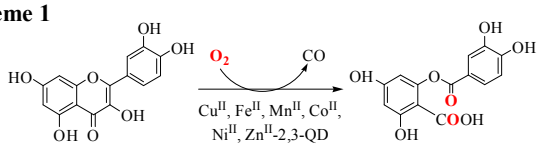

Metal replacement study of 2,3-QD from *Bacillus subtilis* shows that when it was over expressed in *E. coli* in the LB medium with various M^{II} (M = Mn, Fe, Co, Ni, Cu, Zn) salts, the highest and next highest reactivity was found for Mn(II)- and Co(II)-substituted 2,3-QD.[14a] Interestingly, however, the 2,3-QD from *Streptomyces* sp. FLA is most active and next active with substituted by Ni(II)- and Co(II) ion.[14b,c] These results clearly indicate that the enzymatic activity is remarkably influenced by the metal ion and emphasize the importance of the metal ion in the catalytic role of 2,3-QD, in other words, 2,3-QD is a "promiscuous" enzyme and has surprising variability in metal cofactor selectivity. It is similar to other enzyme systems such as acireductone dioxygenase (Fe, Ni, Co, Mn and Mg)[15a] and extra-

Department of Chemistry, Dalian University of Technology, Linggong Road 2, 116024, Dalian, China. E-mail: yingjis@dlut.edu.cn
Fax: +86 411 8498 6040; Tel: +86 411 8498 6040

† Electronic Supplementary Information (ESI) available: The X-ray structure determinations, reaction products analysis data, kinetic data, MS, FT-IR, CV, LC-MS spectra, Eyring plot, and crystallographic information (CIF) CCDC 969850 for **2A**, 969852 for **3A**, 969853 for **4A**, 969854 for **5** and 969851 for **2B**, respectively. For ESI and crystallographic data in CIF or other electronic format see DOI: 10.1039/b000000x/

diol catechol dioxygenase (Fe, Co and Mn).[15b] The metal diversity among various kinds of dioxygenases for catalysis and the variability in metal cofactor selection in the same dioxygenase are a very magnetic, incomprehensible and unclear field, and they rise our interest and question that how O_2 activation and C–C bonds cleavage can be carried out by the metal center especially by the higher-potential redox-inert Ni^{II} center and non-redox Zn^{II} center in the Ni^{II}- and Zn^{II}-containing dioxygenase.

So far, most of the reported biomimetic studies of 2,3-QD on the catalytic dioxygenation of flavonol were Cu(II)/Cu(I)-complexes.[16-22] With respect to other transition-metal resting 2,3-QD model complexes, only two examples $[Co^{III}(salen)(OH)]$[23] and $[Fe^{III}(O\text{-bs})(salen)]$[24] have been reported. However, the oxidation state of the metal center M(III) and the structures are different from the native enzyme, and $[Fe^{III}(O\text{-bs})(salen)]$ reacted with flavonol and O_2 at elevated temperature (80 − 110 °C).[24] Almost all of the model ligands used in the reported model complexes are *N*-chelating polyamine ligands, and few attention has been paid to the role of active site carboxylate group of Glu. So far, two reports focused on the free carboxylate effects on the reactivity of ES-model complexes of 2,3-QD.[25,26] Addition of excess free carboxylate could accelerate the dioxygenation of the bound substrate flavonolate by coordination with displacement of the carbonyl oxygen atom of flavonolate, in which the coordination mode of flavonolate is changed from bidentate to monodentate. These studies indicate that the coordination of carboxylate is necessary for the catalytic reaction in order to induce reasonable reaction rate as found in the native enzyme.[6] Three types of ligands bearing a carboxylate group were used in the resting 2,3-QD model complexes $[Cu^{II}(BPEA)Obs]$ (BPEA = *N*,*N*-bis(2-pyridylmethyl) amino-2-ethanoate, Obs: *O*-benzoylsalicylic acid),[17a] $[Cu^{II}LCl]$ (L = 1-benzyl-4-acetato-1,4,7-triazacyclononane),[21] and $[Cu^{II}(11a\text{-}H)]_2(PF_6)_2$ (11a-H = 2-{5-[bis-(2-isopropyl-3-methyl-3H-imidazol-4-yl)-methyl]-1-methyl-1H-imidazol-2-yl}-2-methyl-propionic acid),[22] but the effect of the introduced carboxylate group on the reactivity was not observed in these complexes.

In a word, the precise roles of the metal ion and the carboxylate group of Glu as well as the catalytic mechanism of 2,3-QD are not clear yet, and there are no series of the divalent first row M^{II} ion complexes have been reported as various M^{II}-substituted resting 2,3-QD models yet. In order to gain further insights into the effects of metal ion as well as the carboxylate group of Glu on the chemical functions of 2,3-QD, we herein prepared and characterized a series of the carboxylate ligand supported transition metal complexes $[M^{II}L(OAc)]$ (M = Mn (**1**), Fe (**2**), Co (**3**), Ni (**4**), Cu (**5**) and Zn (**6**); **LH** = 2-{[bis(pyridine-2-ylmethyl)amino]methyl}-4-methoxy benzoic acid) (Fig. 1)) as structural and functional models of various M^{II}-substituted resting 2,3-QD.

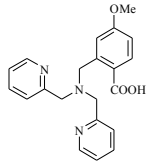

Fig. 1 Structure of ligand **LH**.

Results and discussion

Synthesis and structural characterization.

The model complexes $[M^{II}L(OAc)]$ (M = Mn (**1**), Fe (**2**), Co (**3**), Ni (**4**), Cu (**5**) and Zn (**6**)) were synthesized by treating 1 eq. neutral ligand **LH** and the corresponding $M^{II}(OAc)_2{\cdot}nH_2O$ (n = 0 for Fe^{II} and 4 for others) in CH_3OH under N_2 without adding any base. In these cases, the acetate anion OAc^- of $M^{II}(OAc)_2$ may act as a base to accept the carboxylic acid proton of **LH**.

For the Cu^{II}-complex, blue X-ray-quality single crystal of mononuclear $[Cu^{II}L(OAc)]{\cdot}0.5CH_3OH{\cdot}1.5H_2O$ (**5**) (Fig. 2d) was obtained successfully. While for other complexes $[M^{II}L(OAc)]$ (M = Fe (**2**), Co (**3**) and Ni (**4**)), we only obtained ligand carboxylate bidentate bridged dimer structures $[Fe^{II}LCl]_2{\cdot}4.5H_2O$ (**2A**) (Fig. 2a), $[Co^{II}LCl]_2{\cdot}4H_2O$ (**3A**) (Fig. 2b) and $[Ni^{II}L(CH_3OH)]_2Cl_2{\cdot}3.5H_2O$ (**4A**) (Fig. 2c), respectively, with displacement of the co-ligand OAc^- by additional coordination of Cl^- (from the solvent CH_2Cl_2) or solvent CH_3OH during crystallization of the corresponding mononuclear complexes $[M^{II}L(OAc)]$. Summary of the crystallographic data acquisition and refinement parameters are shown in Table 1, and the selected bond distances and angles are listed in Table 2.

The structure of $[Cu^{II}L(OAc)]{\cdot}0.5CH_3OH{\cdot}1.5H_2O$ (**5**) comprises two crystallographically inequivalent molecules, which are different from each other slightly only in the bond lengths and angles. Each Cu(II) center exhibits a distorted square pyramidal geometry (τ = 0.20/0.24) consisting of one oxygen atom O(1/1A) (carboxylate of L^-) and three nitrogen atoms from ligand L^-, and one oxygen atom O(4/4A) from the co-ligand OAc^-, where O(1/1A) occupies the axial position. The Cu(1/1A)–O(1/1A) distance is 2.1351(17)/2.1471(16) Å, which is slightly longer than those of the Cu(II)-containing 2,3-QD (2.10 Å) from *Aspergillus japonicus*[6] and other model complexes such as $[Cu^{II}(BPEA)(O\text{-bs})]$ (1.972(2) Å),[17a] $[Cu^{II}LCl]$ (1.944(2) Å),[21] and $[Cu^{II}(11a\text{-}H)]_2(PF_6)_2$ (2.0278(13) Å).[22] The Cu(1/1A)–O(4/4A) distance is 1.9473(16)/1.9467(16) Å, which is much shorter than that of the Cu–O_{wat} distance (2.2/2.4 Å) in the *major*/*minor* conformation of Cu-2,3-QD from *Aspergillus japonicus*. The average Cu–N distance is 2.01/2.02 Å, which is slightly shorter than those of the Cu(II)-containing 2,3-QD (2.13 Å) from *Aspergillus japonicus*[6] and other model systems such as $[Cu^{II}(BPEA)(O\text{-bs})]$ (2.11 Å),[17a] $[Cu^{II}LCl]$ (2.11 Å),[21] and $[Cu^{II}(11a\text{-}H)]_2(PF_6)_2$ (2.09 Å).[22]

$[Fe^{II}LCl]_2{\cdot}4.5H_2O$ (**2A**) (Fig. 2a), $[Co^{II}LCl]_2{\cdot}4H_2O$ (**3A**) (Fig. 2b) and $[Ni^{II}L(CH_3OH)]_2Cl_2{\cdot}3.5H_2O$ (**4A**) (Fig. 2c) display a similar ligand carboxylate bidentate bridged dimmer structure. Each metal center of the complexes shows a distorted octahedral geometry, which is coordinated by one carboxylate oxygen O(1), three nitrogen atoms from ligand, another carboxylate oxygen O(2A) from the other ligand and a co-ligand X(1) (X: Cl^- for **2A** and **3A**, or O(4) of solvent CH_3OH for **4A**), where O(1) and X(1) occupy the axial positions. The M–O(1) distance is 2.166(2) Å for **2A**, 2.1379(18) Å for **3A** and 2.0565(13) Å for **4A**, respectively, which is similar to that of the Fe^{II}-containing 2,3-QD (2.10 Å) from *Bacillus subtilis*.[9] The average M–N distance is 2.20 Å for **2A** (similar to that of the Fe^{II}-containing 2,3-QD (2.26 Å) from *Bacillus subtilis*.[9]), 2.16 Å for **3A** and 2.09 Å for **4A**, respectively. The M–X distance is 2.4806(11) Å for **2A**, 2.4680(11) Å for **3A** and 2.1249(16) Å for **4A**, respectively. The bond valence sum (BVS) calculations[27] (2.02 for **2A** and 1.75 for

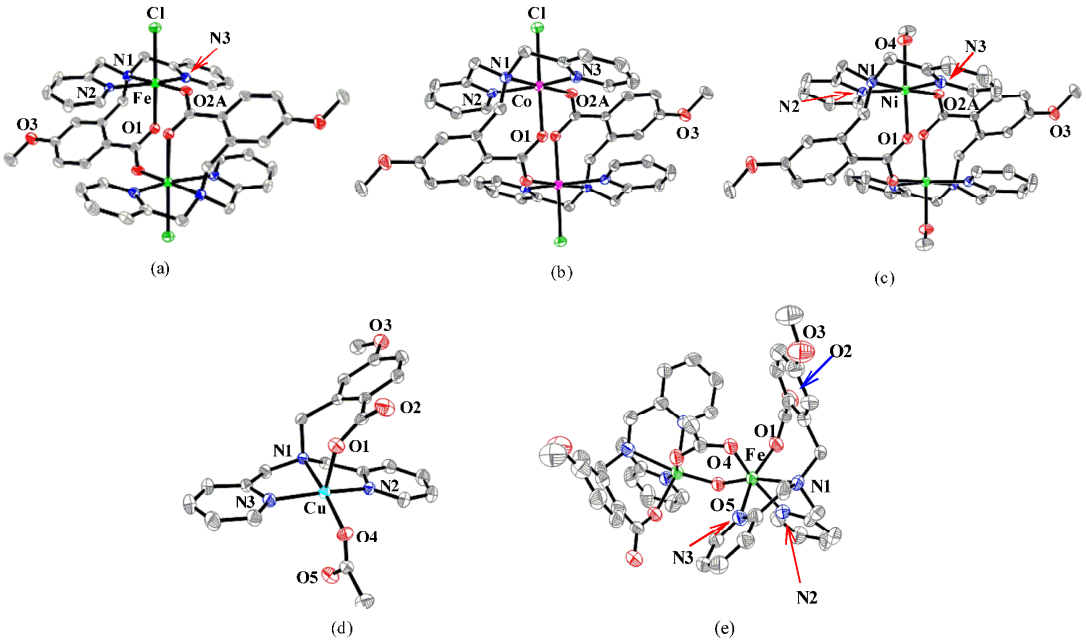

Fig. 2 Thermal ellipsoid drawings (50% probability) of (a) **2A**, (b) **3A**, (c) **4A**, (d) **5** and (e) **2B**. Hydrogen atoms, counter anions and solvent molecules have been omitted for clarity.

Table 1 Summary of X-ray data collection and refinement.

	$[Fe^{II}LCl]_2 \cdot 4.5H_2O$ (**2A**)	$[Co^{II}LCl]_2 \cdot 4H_2O$ (**3A**)	$[Ni^{II}L(CH_3OH)]_2Cl_2 \cdot 3.5H_2O$ (**4A**)	$[Cu^{II}L(OAc)] \cdot 0.5CH_3OH \cdot 1.5H_2O$ (**5**)
Formula	$C_{42}H_{40}Cl_2Fe_2N_6O_6$	$C_{42}H_{40}Cl_2Co_2N_6O_6$	$C_{44}H_{48}Cl_2N_6Ni_2O_8$	$C_{23.5}H_{28}CuN_3O_7$
M_r	907.40	931.56	977.20	528.03
Crystal system	monoclinic	monoclinic	monoclinic	triclinic
Space group	*P*2(1)/*n*	*P*2(1)/*n*	*P*2(1)/*c*	*P*-1
a (Å)	8.736(4)	8.726(5)	13.6889(7)	10.9928(2)
b (Å)	20.255(9)	20.348(11)	13.9132(7)	12.0354(2)
c (Å)	12.610(6)	12.677(7)	15.1302(6)	18.6928(3)
α (°)	90.00	90	90	83.4210(10)
β (°)	95.847(15)	96.148(10)	123.009(3)	78.4230(10)
γ (°)	90.00	90	90	80.3700(10)
V/Å^3	2219.7(18)	2238(2)	2416.5(2)	2380.24(7)
Z	2	2	2	4
D_x /g cm^{-3}	1.358	1.356	1.343	1.473
T/K	296(2)	296(2)	296(2)	296(2)
Crystal habit	block	block	block	block
Crystal color	brwon	purple	light-blue	blue
Crystal size (mm^3)	0.25 × 0.15 × 0.10	0.30 × 0.20 × 0.20	0.15 × 0.12 × 0.10	0.30 × 0.20 × 0.20
μ /mm^{-1}	0.825	0.911	0.944	0.967
$2\theta_{max}$ /deg	50.00	50.00	50.00	50.00
Completeness to θ (%)	98.5	99.8	99.9	99.6
Reflections collected	11635	12698	21800	16089
Independent reflections	3858	3939	4255	8346
R_{int}	0.0430	0.0454	0.0225	0.0199
$R1^a$/w$R2^b$ [I>2sigma(I)]	0.0403/0.0871	0.0369/0.0762	0.0299/0.0729	0.0340/0.0912
$R1^a$/w$R2^b$ (all data)	0.0645/0.0952	0.0534/0.0808	0.0337/0.0758	0.0462/0.0966
Goodness-of-fit (F^2)	1.005	1.001	1.035	1.006

[a] $R1 = \sum || F_o|-| F_c|| / \sum |F_o|$. [b] $wR2 = [\sum w (F_o^2 - F_c^2)^2 / \sum w(F_o^2)^2]^{1/2}$

Table 2 Selected bond distances (Å) and bond angles (deg).

	2A	3A	4A			5	
M–N(1)	2.258(2)	2.194(2)	2.1094(15)	Cu(1)–N(1)	2.0475(18)	Cu(1A) –N(1A)	2.0421(18)
M–N(2)	2.175(2)	2.146(2)	2.0781(17)	Cu(1)–N(2)	1.9845(18)	Cu(1A) –N(2A)	2.0031(19)
M–N(3)	2.162(2)	2.132(2)	2.0779(16)	Cu(1)–N(3)	1.9947(19)	Cu(1A) –N(3A)	2.0060(19)
M–O(1)	2.166(2)	2.1379(18)	2.0565(13)	Cu(1)–O(1)	2.1351(17)	Cu(1A) –O(1A)	2.1471(16)
M–O(2A)	2.000(2)	2.0287(18)	2.0410(13)	Cu(1)–O(4)	1.9473(16)	Cu(1A) –O(4A)	1.9467(16)
M–O(4)/Cl	2.4806(11)	2.4680(11)	2.1249(16)				
O(1)–M–O(2A)	91.59(8)	89.86(8)	90.00(5)	O(1)–Cu(1)–O(4)	93.57(7)	O(1A)–Cu(1A)–O(4A)	90.59(7)
O(1)–M–O(4)/Cl	175.91(5)	177.49(5)	176.21(6)	O(1)–Cu(1)–N(1)	95.04(7)	O(1A)–Cu(1A)–N(1A)	96.14(7)
O(2A)–M–O(4)/Cl	92.12(7)	90.83(6)	86.26(6)	O(1)–Cu(1)–N(2)	100.19(7)	O(1A)–Cu(1A)–N(2A)	104.86(7)
O(1)–M–N(1)	85.52(8)	87.96(8)	91.75(6)	O(1)–Cu(1)–N(3)	96.15(8)	O(1A)–Cu(1A)–N(3A)	92.74(7)
O(1)–M–N(2)	85.60(8)	85.98(7)	89.15(6)	O(4)–Cu(1)–N(1)	171.36(7)	O(4A)–Cu(1A)–N(1A)	173.22(7)
O(1)–M–N(3)	89.15(8)	90.53(7)	94.53(6)	O(4)–Cu(1)–N(2)	95.97(7)	O(4A)–Cu(1A)–N(2A)	96.08(8)
O(2A)–M–N(1)	173.40(8)	173.86(8)	173.59(6)	O(4)–Cu(1)–N(3)	95.17(8)	O(4A)–Cu(1A)–N(3A)	95.56(8)
O(2A)–M–N(2)	98.56(9)	96.52(8)	93.54(6)	N(1)–Cu(1)–N(2)	83.24(7)	N(1A)–Cu(1A)–N(2A)	82.95(7)
O(2A)–M–N(3)	110.79(9)	108.20(8)	105.48(6)	N(1)–Cu(1)–N(3)	83.18(8)	N(1A)–Cu(1A)–N(3A)	83.39(7)
O(4)/Cl–M–N(1)	90.61(7)	91.10(7)	92.03(6)	N(2)–Cu(1)–N(3)	159.56(8)	N(2A)–Cu(1A)–N(3A)	158.73(8)
O(4)/Cl–M–N(2)	92.16(7)	91.54(6)	91.64(7)				
O(4)/Cl–M–N(3)	91.13(6)	91.54(6)	85.93(7)				
N(1)–M–N(2)	75.32(9)	77.60(8)	80.33(6)				
N(1)–M–N(3)	75.15(9)	77.57(8)	80.53(6)				
N(2)–M–N(3)	150.32(9)	155.03(8)	160.61(7)				

3A, respectively) prove that the oxidation state of the metal center in both of **2A** and **3A** are +2, which is in good agreement with the ESI-MS and EPR results described below.

Since the mononuclear Fe^{II}-complex $[Fe^{II}L(OAc)]$ (**2**) is so air sensitive in solution, we also obtained an auto-oxidized μ-oxo, μ-OAc diiron(III) structure $[(Fe^{III}L)_2(\mu\text{-O})(\mu\text{-OAc})]Cl\cdot 10H_2O$ (**2B**) (Fig. 2e, ESI, Table S1 and S2) during crystallization. In **2B**, each oxidized Fe^{III} center is coordinated by one carboxylate oxygen O(1), three nitrogen atoms of ligand, two oxygen atoms O(5) (μ-oxo) and O(4) (μ-OAc) to form a distorted octahedral geometry, in which O(5) and N(2) (one of the pyridine nitrogen atoms) are at the axial positions. The Fe(1)–O(1) distance is 1.985(5) Å, which is much shorter than those of $[Fe^{II}LCl]_2\cdot 4.5H_2O$ (**2A**) (2.166(2) Å) and the Fe^{II}-containing resting 2,3-QD (2.10 Å) from *Bacillus subtilis*.[9] The average Fe–N distance (2.20 Å) is close to that of $[(6\text{-}Ph_2TPAFe^{III}(fla))_2(\mu\text{-O})](ClO_4)_2$ (2.21 Å)[28] but slightly shorter than that of the Fe^{II}-containing resting 2,3-QD (2.26 Å) from *Bacillus subtilis*.[9] The Fe(1)–O(5) (μ-oxo) distance (1.804(3) Å) is similar to that of $[(6\text{-}Ph_2TPAFe^{III}(fla))_2(\mu\text{-O})](ClO_4)_2$ (1.7890(14) Å).[28] These results indicate that the oxidation state of each Fe ion in **2B** is +3, which is consistent with the BVS calculated valence[27] of the Fe ion (2.95) and the ESI-MS results described below.

Though the mononuclear X-ray-quality single crystals of **1** − **4** and **6** were not obtained, based on other spectroscopic results such as FT-IR, ESI-MS and EPR results described below, we suggest that the complexes **1** − **4** and **6** also have a similar mononuclear structure with a co-ligand OAc^- bidentate coordinated distorted octahedral geometry.

Spectroscopic and redox properties of complexes

FT-IR Spectroscopy. In both of the solid and solution states, each complex shows two vibrations $\nu_{as}(COO^-)$ and $\nu_s(COO^-)$ of the carboxylate group of L^- at 1594 − 1610 cm^{-1} and 1390 − 1417 cm^{-1}, respectively (Table 3 and ESI, Table S3 and Fig. S2 for **4**). Both vibrations are red-shifted relative to that of free ligand LH (1688 and 1601 cm^{-1}, respectively). The difference between them ($\Delta\nu = \nu_{as}(COO^-) - \nu_s(COO^-)$) is 181 − 214 cm^{-1}, rendering a monodentate binding mode of the carboxylate group of L^- for all complexes in both states.[29,30] In addition, two vibrations $\nu_{as}(COO^-)$ and $\nu_s(COO^-)$ of the co-ligand OAc^- appeared at 1549 − 1583 cm^{-1} and 1379 − 1440 cm^{-1}, respectively. For $[Cu^{II}L(OAc)]$ (**5**), the $\Delta\nu$ is 193 and 197 cm^{-1} in the solid and solution state, respectively, indicating that OAc^- was monodentate coordinated in both states,[29,30] which is consistent with the X-ray structure shown in Fig. 2d. For other complexes **1** − **4** and **6**, the $\Delta\nu$ is 143 − 158 cm^{-1} and we did not observed any vibration of $\nu(COO^-)$ of free acetate near 1700 cm^{-1}, indicating that the co-ligand OAc^- was bidentate coordinated in both states.[29,30] All these lead up to the conclusion that all of the complexes $[M^{II}L(OAc)]$ keep a mononuclear structure even in solution, which is in good agreement with the ESI-MS and solution EPR results described below.

UV-vis Spectroscopy. Electronic absorption spectra of **1** − **6** were recorded in DMF solution (Table 3). Each complex exhibits an intense absorption band at about 265 nm, which can be assigned to the transition band of the model ligand. All of the complexes except **1** and **6** also exhibit 1 − 3 weak absorption bands in the visible region, which can be assigned to the spin-allowed d-d transition bands in the ligand field.

$[Fe^{II}L(OAc)]$ (**2**) exhibits one relatively strong band at 15873 cm^{-1}, which can be assigned to the spin-allowed d-d transition band of Fe^{II} ($3d^6$) in the distorted octahedral ligands field.

$[Co^{II}L(OAc)]$ (**3**) exhibits two shoulder bands at 16807 and 20080 cm^{-1}, respectively, which can be assigned to the spin-allowed d-d transition bands of Co^{II} ($3d^7$) in the distorted octahedral ligands field, ν_2 ($^4A_{2g} \leftarrow {}^4T_{1g}(F)$) and ν_3 ($^4T_{1g}(P) \leftarrow {}^4T_{1g}(F)$), respectively. The ligands-field constants Dq (897 cm^{-1})

and B (892 cm^{-1}) were calculated[31] by using the observed bands ν_2 and ν_3. The B value is smaller than that of free Co^{II} ion (1030 cm^{-1}).

[Ni^{II}L(OAc)] (**4**) exhibits three weak bands at 10417, 16393 and 26316 cm^{-1}, respectively, which can be assigned to the spin-allowed d-d transition bands of Ni^{II} ($3d^8$) in the distorted octahedral ligands field, ν_1 ($^3T_{2g} \leftarrow {}^3A_{2g}$), ν_2 ($^3T_{1g}(F) \leftarrow {}^3A_{2g}$) and ν_3 ($^3T_{1g}(P) \leftarrow {}^3A_{2g}$), respectively. The ligands-field constants Dq (1042 cm^{-1}) and B (764 cm^{-1}) were also calculated[31] by using the observed bands ν_1, ν_2 and ν_3. The B value is smaller than that of free Ni^{II} (1040 cm^{-1}).

[Cu^{II}L(OAc)] (**5**) exhibits one weak broad band at 14925 cm^{-1}, which can be assigned to the three overlapped spin-allowed d-d transition bands of Cu^{II} ($3d^9$) in the distorted square pyramidal ligands field.

ESI-MS spectroscopy. The solution structure of the complexes was also examined by ESI-MS. Each model complex [M^{II}L(OAc)] (M = Mn, Co, Ni, Cu and Zn) exhibits two peak clusters [M^{II}L(OAc)]H^+ and [M^{II}L]$^+$ (Table 3 and ESI, Fig. S1), indicating that the co-ligand OAc^- is easily displaced by the substrate flavonol to form the corresponding ternary complex [M^{II}L(fla)] during the catalytic dioxygenation reaction of flavonol, which is consistent with the titration results described bellow. Since the Fe(II)-complex [Fe^{II}L(OAc)] (**2**) is so air sensitive, we observed the peak clusters of the iron(II) complexes and the partly auto-oxidized iron(III) complexes at *m*/*z* (pos.) = 418.1 ([$Fe^{II}L]^+$), 450.1 ([$Fe^{II}L(CH_3OH)]^+$), 477.0 ([$Fe^{III}L(OAc)]^+$) and 911.1 ([$(Fe^{III}L)_2(OAc)(O)]^+$) (Table 3 and ESI, Fig. S1b). For other complexes, we did not observe any dimmer or oxidazed peak clusters. The *m*/*z* value and the isotope distribution pattern of each peak cluster is in excellent agreement with the calculated value, indicating that each complex [M^{II}L(OAc)] remains its mononuclear structure and oxidation state in solution except [Fe^{II}L(OAc)] (**2**), which is consistent with the solution FT-IR and solution EPR results.

Magnetic properties. The X-band EPR spectra of the complexes **1**, **2, 3** and **5** in the absence and presence of 1 eq. flaH were examined under N_2 at 100 K. In order to further prove the solution structure, oxidation state and spin state of the metal ion, we tried our best to examine the solution magnetic susceptibility of the complexes by NMR using Frei-Bernstein's method. Unfortunately, the NMR spectrum could not be recorded because of the failed tuning both by automatically and manually.

The spectrum of [Mn^{II}L(OAc)] (**1**) displays a strong 6-fold hyperfine splitting centered at g = 2.00 with a hyperfine coupling constant A = 92 G (Fig. 3a-A), similar to that of the native Mn^{II}-containing enzyme (g = 2.0, A = 93 G) and its ES adduct from *B. subtilis*,[14a] suggesting that [Mn^{II}L(OAc)] (**1**) exhibits a typical mononuclear distorted octahedral coordination geometry with nitrogen and oxygen donors.[32] In the presence of 1 eq. substrate flavonol (flaH) under N_2 and after the catalytic dioxygenation reaction, the signal did not exhibit obvious changes with the EPR parameter of g = 2.02 (A = 90 G) (Fig. 3a-B) and g = 2.01 (A = 94 G) (Fig. 3a-C), respectively, reflecting that [Mn^{II}L(OAc)] (**1**) did not change the oxidation state during the catalytic dioxygenation reaction, which coincide in the ESI-MS and CV results.

In the absence (Fig. 3b-A) and presence (Fig. 3b-B) of 1 eq. flaH under N_2, [Fe^{II}L(OAc)] (**2**) are all EPR silent. In order to confirm the spin state of Fe(II) in **2**, the magnetic susceptibility of **2** in solid state was measured at room temperature (300 K). The magnetic moments of **2** in solid state is calculated and it is 4.47 μ_B, which is a little smaller than the calculated value using the spin-only equation of the high-spin Fe^{II} (4.90 μ_B), implying that the spin state of Fe(II) of **2** in solid state is high-spin. After the dioxygenation reaction, a typical mononuclear Fe(III) signal at g

Table 3 Summary of spectroscopic and CV data for the complexes.

Complex	[Mn^{II}L(OAc)] (**1**)	[Fe^{II}L(OAc)] (**2**)	[Co^{II}L(OAc)] (**3**)	[Ni^{II}L(OAc)] (**4**)	[Cu^{II}L(OAc)] **(5)**	[Zn^{II}L(OAc)] **(6)**
FT-IR, ν_{as}/ν_s (COO^- of L)	1602/1413	1606/1396	1596/1397	1605/1417	1610/1410	1604/1390
$\Delta\nu$	189	210	199	188	200	214
ν_{as}/ν_s (COO^- of OAc^-)	1557/1402	1557/1402	1570/1420	1550/1392	1574/1381	1583/1439
$\Delta\nu$	155	155	150	158	193	144
UV-vis, nm (ε, M^{-1} cm^{-1})	265 (23449)	265 (25018) 630 (44)	266 (28395) 498 (71) 595 (37)	268 (28214) 380 (154) 610 (47) 960 (71)	266 (27483) 670 (53)	267 (7677)
ESI-MS, *m*/*z*	417.3 ([$Mn^{II}L]^+$) 477.5 ([Mn^{II}L(OAc)]H^+)	418.1 ([$Fe^{II}L]^+$) 477.0 ([Fe^{III}L(OAc)]$^+$) 911.1 ([$(Fe^{III}L)_2(OAc)(O)]^+$)	421.0 ([$Co^{II}L]^+$) 481.2 ([Co^{II}L(OAc)]H^+)	420.0 ([$Ni^{II}L]^+$) 480.2 ([Ni^{II}L(OAc)]H^+)	425.0 ([$Cu^{II}L]^+$) 485.0 ([Cu^{II}L(OAc)]H^+)	426.2 ([$Zn^{II}L]^+$) 486.3/508.3 ([Zn^{II}L(OAc)]H/Na^+)
EPR	g = 2.01 A = 92 G	silent			g_1 = 2.23 g_2 = 2.05 g_3 = 2.01 A = 170 G	
CV, $E_{1/2}$ (V)		–0.110 ($Fe^{III/II}$)	–0.169 ($Co^{III/II}$)		–0.462 ($Cu^{II/I}$)	
ΔE_p (mV)		118	71		106	
i_{pc}/i_{pa}		0.22	0.90		1.05	
$E_{1/2}$ (V) (+ 1 eq. flaH)		–0.099 ($Fe^{III/II}$)	–0.169 ($Co^{III/II}$)		–0.440 ($Cu^{II/I}$)	
ΔE_p (mV)		82	70		110	
i_{pc}/i_{pa}		0.99	0.88		0.81	
$E_{1/2}$ ($fla^{\bullet}/fla^-$) (V)	+0.361	+0.149	+0.270		+0.384	
$E_{pa/}$ E_{pc}	+0.417/+0.304	+0.179/+0.118	+0.315/+0.225	+0.326	+0.460/+0.307	+0.396
ΔE_p (mV)	78	61	90		153	
i_{pc}/i_{pa}	0.43	0.63	0.82		0.86	

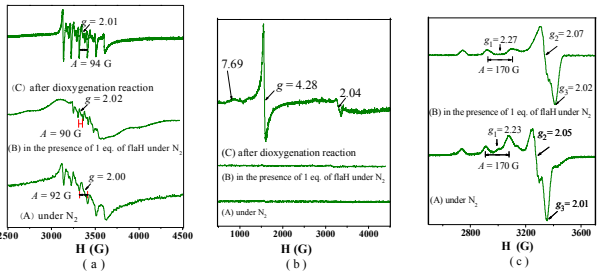

Fig. **3** EPR spectra of (a) [Mn^{II}L(OAc)] (**1**), (b) [Fe^{II}L(OAc)] (**2**) and (c) [Cu^{II}L(OAc)] (**5**). (A) under N_2, (B) in the presence of 1 eq. flaH under N_2, (C) after dioxygenation reaction.

= 7.69, 4.28 and 2.04 (Fig. 3b-C) appeared, indicating that the oxidation state of Fe(II) was changed during the catalytic dioxygenation reaction, which is in line with the ESI-MS and CV results.

The EPR signals of [Co^{II}L(OAc)] (**3**) in the absence and presence of 1 eq. flaH at the liquid nitrogen temperature (100 K) is too weak to be analyzed in detail (ESI, Figure S3-A and B, respectively).

Complex [Cu^{II}L(OAc)] (**5**) exhibits a typical 4-fold hyperfine splitting mononuclear Cu^{II} ($3d^9$) signal with the EPR parameters of g_1 = 2.23 (A = 170 G), g_2 = 2.05 and g_3 = 2.01 (Fig. 3c-A), which is close to that of the Cu(II)-containing 2,3-QD from *Aspergillus niger* DSM 821 (g_1 = 2.29, A = 150 G, g_2 = 2.06, g_3 = 2.01, square pyramidal geometry).[8] The observed g values ($g_1 > g_2 > g_3$) are typical for a Cu^{II} ion with the unpaired electron lying in the d_{x2-y2} orbital at the ground state.[33-35] After adding 1 eq. flaH under N_2, we only observed slight change on the EPR parameters of g_1 = 2.27 (A = 170 G), g_2 = 2.07 and g_3 = 2.02 (Fig. 3c-B), which are similar to that of the enzyme-flavonol adduct ($g_{//}$ = 2.31, $A_{//}$ = 142 G) from *A. japonicus*.[36]

Electrochemistry. The redox properties of the complexes [M^{II}L(OAc)] in the absence and presence of 1 eq. substrate flaH were examined by cyclic voltammetry under N_2 at room temperature. The results are summarized in Table 3, Fig. 4 and ESI, Fig. S4. All potentials are reported *vs.* SCE.

There is a quasi-reversible redox couple corresponding to one-electron oxidation from M(II) to M(III) at $E_{1/2}$ = –0.110 V (ΔE_p = 118 mV, i_{pc}/i_{pa} = 0.22) for [Fe^{II}L(OAc)] (**2**) (ESI, Fig. S4a) and $E_{1/2}$ = –0.169 V (ΔE_p = 71 mV, i_{pc}/i_{pa} = 0.90) for [Co^{II}L(OAc)] (**3**) (ESI, Fig. S4b), respectively. For [Cu^{II}L(OAc)] (**5**), a quasi-reversible redox couple appeared at $E_{1/2}$ = –0.462 V (ΔE_p = 106 mV, i_{pc}/i_{pa} = 1.05) (ESI, Fig. S4c), which can be assigned to one-electron reduction of Cu^{II} to Cu^{I}. Such a metal ion redox couple was not observed in the Mn^{II}-, Ni^{II}- and Zn^{II}-complexes even under O_2 over the range of –2.0 V − +2.5 V. Maybe it is due to high oxidation potential and stability of the Mn^{II} and Ni^{II} in our model system resulting in hard to be oxidized to M^{III}, and the Zn^{II} is a non-redox metal ion. These results indicate that the Mn^{II}-, Ni^{II}- and Zn^{II}-complexes are relatively stable in solution and remaining their oxidation state during the catalytic dioxygenation reaction, which is in line with the ESI-MS and EPR results.

When a DMF solution of 1 eq. substrate flavonol was added to the DMF solution of [M^{II}L(OAc)] under N_2, we also observed a quasi-reversible one-electron redox couple of Fe^{II}/Fe^{III} (Fig. 4),

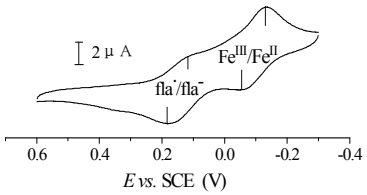

Fig. **4** Cyclic voltammogram of [Fe^{II}L(OAc)] (**2**) in the presence of 1 eq. substrate flavonol in DMF when contacted slowly with O_2.

Co^{II}/Co^{III} and Cu^{II}/Cu^{I} (Table 3). The $E_{1/2}$ value of these redox couples did not show notable change and they are the same with that of the corresponding ES model complex [Co^{II}L(fla)] (–0.169 V)[37] and similar to those of the non-substituted analogue [$M^{II}L^{H}$(fla)] (M = Fe, Co, Cu; $L^{H}H$ = 2-{[bis(pyridin-2-ylmethyl)amino]methyl} benzoic acid) (Fe: –0.094 V, Co: –0.062 V, Cu: –0.427 V, respectively)[38] but more negative than that of the corrosponding non-carboxylate analogue ligand complex [(6-Ph_2TPA)Fe^{II}(fla)]OTf (+0.35 V),[28] due to the existing negative charge of carboxylate in our model ligand system L^- by electron donation.

Interestingly, when the above solution was contacted slowly with O_2, a new quasi-reversible redox couple appeared at $E_{1/2}$ = +0.361 V (E_{pa} = +0.417 V, ΔE_p = 78 mV, i_{pc}/i_{pa} = 0.43) for **1** (ESI, Fig. S4d), +0.149 V (E_{pa} = +0.179 V, ΔE_p = 61 mV, i_{pc}/i_{pa} = 0.63) for **2** (Fig. 4), +0.270 V (E_{pa} = +0.315 V, ΔE_p = 90 mV, i_{pc}/i_{pa} = 0.82) for **3** (ESI, Fig. S4e) and +0.384 V (E_{pa} = +0.460 V, ΔE_p = 153 mV, i_{pc}/i_{pa} = 0.86) for **5** (ESI, Fig. S4g), respectively. In fact, a new absorption band appeared at 670 nm (the same with the reported free flavonoxy radical fla$^{\bullet}$ at 676 nm[38,39]) during the reaction of flavonol with O_2 in the presence of 1 eq. [M^{II}L(OAc)] (Fig. 6-red line for **1**), which could be assigned to the flavonoxy radical fla$^{\bullet}$ generated in a one-electron oxidation of fla$^-$. While for [Ni^{II}L(OAc)] (**4**) and [Zn^{II}L(OAc)] (**6**), we only observed an irreversible oxidation wave at E_{pa} = +0.326 V and +0.396 V (ESI, Fig. S4f and S4h), respectively. The reported potassium flavonolate only exhibits an oxidation wave (from fla$^-$ to fla$^{\bullet}$) but no reduction wave (from fla$^{\bullet}$ to fla$^-$) because of its lower stability of the generated free fla$^{\bullet}$.[39] The presence of a reverse reduction wave of fla$^{\bullet}$ → fla$^-$ in the presence of our model complexes indicates that the coordinated fla$^{\bullet}$ in our model system is more stable than that of free fla$^{\bullet}$, namely, the metal ion could stabilize the fla$^{\bullet}$ by delocalization of the unpaired electron. The E_{pa} of the coordinated flavonolate are the same with the corresponding ES model complexes [Co^{II}L(fla)] (+0.315 V)[37] and Ni^{II}L(fla)] (+0.326 V),[40] and a little negative than those of the non-substituted analogue [$M^{II}L^{H}$(fla)] (M = Mn, Fe, Co, Ni and Zn) (Mn: +0.469 V, Fe: +0.169 V, Co: +0.396 V, Ni: +0.401 V and Zn: +0.438 V, respectively)[38] but much negative than those of the corresponding non-carboxylate ligand complexes [M^{II}(6-Ph_2TPA)(fla)]OTf (M = Mn, Ni, Cu and Zn) (in CH_2Cl_2) (Mn: +0.765 V, Ni: +0.906 V, Cu: +1.06 V and Zn: +0.934 V, respectively),[28] [Fe^{II}(fla)$(H_2O)_4$]Cl (+0.84 V) and [Cu^{II}(fla)$(H_2O)_2$]Cl (+0.87 V) (in MeOH),[41] due to the existing negative charge of carboxylate in our supporting model ligand L^-, which could increase the electron density of flavonate via the metal ion and O(carbonyl)=C(4)−C(3)=C(2) "electron conduit"

as found in the enzyme systems[6,13,14] and other model systems.[37,40] Namely, the bound substrate flavonolate are more easily oxidized in our model system, resulting in higher catalytic activity of the model complexes [M^{II}L(OAc)] on the oxygenative degradation of flavonol as described below.

The E_{pa} of the coordinated flavonolate is in the range of +0.179 − +0.460 V (over a range of 281 mV) and in the order of Fe (**2**) (+0.179 V) < Co (**3**) (+0.315 V) < Ni (**4**) (+0.326 V) < Zn (**6**) (+0.396 V) < Mn (**1**) (+0.417 V) < Cu (**5**) (+0.460 V), implying that the E_{pa} of the bound substrate flavonolate are sensitive to the metal ion, which could tune the electron density of the substrate flavonol by coordination via O(carbonyl)=C(4)−C(3)=C(2) "electron conduit" as found in the enzyme systems[6,13,14] and other model systems.[37,40]

Catalitic dioxygenation of flavonol by the complexes [M^{II}L(OAc)] (Enzymatic reactivity). The dioxygenation of flavonol catalyzed by [M^{II}L(OAc)] (5.0% molar ratio relative to the substrate flavonol) in DMF at 70/100 °C give *O*-benzoylsalicylic acid (HObs) (*m*/*z* (pos.): 260.1 $(M + NH_4)^+$) (0 − 27.2%) and CO (over 15% for **3**) as the primary products (ESI, Table S4, Fig. S5 and S6). The HObs was then hydrolyzed with small amount of water in the solvent and amidated by the solvent DMF to give benzoic acid (*m*/*z* (neg.): 121.3 $(M - H)^-$, 181.1 $(M + OAc)^-$ (25.4 − 82.4%), salicylic acid (*m*/*z* (neg.): 137.2 $(M - H)^-$) (55.1 − 81.3%), *N*,*N*-dimethylbenzamide (*m*/*z* (pos.): 150.2 $(M + H)^+$) (0 − 36.8%) and 2-hydroxy-*N*,*N*-dimethyl-benzamide (*m*/*z* (pos.): 166.2 $(M + H)^+$) (0 − 9.40%) (characterized by LC-MS and NMR, Scheme 2 and ESI, Table S4, Fig. S5 and S7). The dioxygenation reaction products of the substrate flavonol catalyzed by our model complexes [M^{II}L(OAc)] are very similar to that of the reaction products catalyzed by the native 2,3-QD, indicating that our model complexes [M^{II}L(OAc)] have enzymatic reactivity toward flavonol and O_2. The TON and conversion rate of the complexes (ESI, Table S4) show some differences and it is almost in a metal ion dependent order, which is consistent with the kinetic results described bellow.

Scheme 2. Dioxygenation of flavonol catalyzed by the model complexes [M^{II}L(OAc)] and their reaction products.

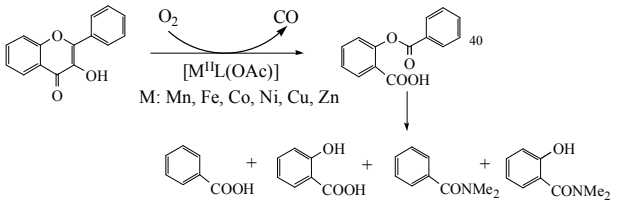

Detailed kinetic measurements for dioxygenation of substrate flavonol catalyzed by the model complexes [M^{II}L(OAc)] were carried out in DMF at 55 – 100 °C with a ratio between initial concentrations of [M^{II}L(OAc)] and flavonol in the range of 1:20 – 1:200. The catalytic dioxygenation reactions were followed by monitoring the absorption changes of the substrate flavonol at 343 nm (log ε = 4.24) (Fig. 5a for [Co^{II}L(OAc)] (**3**)). Experimental conditions and the obtained initial rates are summarized in Table S5 (ESI). The activation parameters are calculated from an Eyring plot (ESI, Fig. S8) and an Arrhenius plot, and summarized in Table 4. The plots of the initial reaction rate *vs.* all of the initial concentrations of [M^{II}L(OAc)] (Fig. 5b),

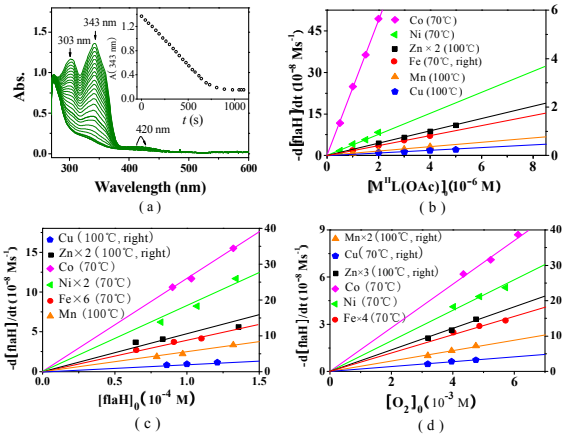

Fig. 5 (a) Spectral changes accompanying the [Co^{II}L(OAc)] (**3**)-catalyzed dioxygenation of flavonol during the experiment 1 in Table S4. Inset: Time course of the absorption changes of flavonol at 343 nm. Plots of –d[flaH]/d*t* *vs.* (b) $[M^{II}L(OAc)]_0$, (c) $[flaH]_0$ and (d) $[O_2]_0$.

flavonol (Fig. 5c) and O_2 (Fig. 5d) are linear, respectively. So the rate law can be described as –d[flaH]/dt = k[flaH][M^{II}L(OAc)][O_2]. The third reaction rate constants k for the complexes [M^{II}L(OAc)] were thus determined as 5.51 − 579 × 10^3 M^{-2} s^{-1} ($\Delta H^{\neq}$ = 31 − 43 kJ mol^{-1}, $\Delta S^{\neq}$ = −47 − −64 J mol^{-1} K^{-1}) (Table 4, ESI, Table S5 and Fig. S8) at 70 °C (for the Fe^{II}-, Co^{II}- and Ni^{II}-complexes) or 100 °C (for the Mn^{II}-, Cu^{II}- and Zn^{II}-complexes). The catalytic reactivity of the previously reported 2,3-QD model complexes were lower and required higher temperature (80 − 139 °C) (Table 4). One example of the catalytic dioxygenation reactions were carried out at a temperature range of 40 – 90°C,[21] but only a turnover rate of 6 h^{-1} at 90°C rather than detail rate constants data at lower temperature were reported and the reaction main products are not the enzymatic reaction products of the native 2,3-QD. However, our model complexes show higher enzymatic activity at lower temperature (55 − 100 °C) especially [Co^{II}L(OAc)] (**3**) and [Ni^{II}L(OAc)] (**4**) (k = 57.9 × 10^4 M^{-2} s^{-1} and 9.53 × 10^4 M^{-2} s^{-1} at 70 °C, respectively), presumably due to the existing carboxylate group in the supporting model ligand. The role of the carboxylate group is to lower the redox potential of the bound substrate flavonolate by electron donation via the metal ion and O(carbonyl)=C(4)−C(3)=C(2) "electron conduit" as found in the enzyme systems[6,13,14] and other model systems,[37,40] providing important insights into the role of Glu in 2,3-QD. Thus, our model complexes are a series of structural and functional models for the active site of various M^{II}-substituted resting 2,3-QD.

The complexes show strikingly different reactivity on the catalytic dioxygenation of the substrate flavonol and it is in a metal ion dependent order of Co (**3**) > Ni (**4**) > Zn (**6**) > Fe (**2**) > Mn (**1**) > Cu (**5**), which is just contrary to the order of the oxidation potential of the coordinated flavonolate (Fe (**2**) < Co (**3**) < Ni (**4**) < Zn (**6**) < Mn (**1**) < Cu (**5**)) except the Fe^{II}-complex [Fe^{II}L(OAc)] (**2**). The reactivity order inconformity of [Fe^{II}L(OAc)] (**2**) maybe due to the formation of the less active μ-oxo diiron(III) complex [$(Fe^{III}L)_2(\mu$-O)(μ-OAc)]Cl (**2B**) during the catalytic reaction.

Table 4 The kinetic data and the activation parameters for the dioxygenation of flavonol in DMF.

	T (°C)	k (10^3 M^{-2} s^{-1})	$\Delta H^{\neq}$ (kJ mol^{-1})	$\Delta S^{\neq}$ (J mol^{-1} K^{-1})	E_a (kJ mol^{-1})	*Ref.*
$[Mn^{II}L(OAc)]$ (**1**)	100	16.5 ± 0.12	41 ± 5	–56 ± 3	44 ± 8	This work
$[Fe^{II}L(OAc)]$ (**2**)	70	5.51 ± 0.02	38 ± 2	–64 ± 2	40 ± 3	This work
$[Fe^{III}$(O-bs)(salen)]	110	48.2 ± 0.15	50 ± 2	–27 ± 4	53 ± 2	[24]
$[Co^{II}L(OAc)]$ (**3**)	70	579 ± 0.08	31 ± 3	–47 ± 3	33 ± 4	This work
$[Ni^{II}L(OAc)]$ (**4**)	70	95.3 ± 0.07	35 ± 5	–47 ± 6	39 ± 4	This work
$[Cu^{II}L(OAc)]$ (**5**)	100	13.5 ± 0.12	43 ± 7	–51 ± 10	47 ± 8	This work
$[Cu^{II}$(fla)(idpa)]ClO_4	130	0.422 ± 0.15	71 ± 6	– 97 ± 15	——	[18]
$[Cu^{II}(fla)_2]$	120	2.02 ± 0.07	139 ± 5	168 ± 13	142 ± 6	[20]
$[Zn^{II}L(OAc)]$ (**6**)	100	45.2±0.03	37±2	-58±2	40±3	This work

In order to prove the above postulation, the μ-oxo diiron(III) complex **2B** was titrated by the substrate flavonol and the kinetic study of the dioxygenation of flavonol catalyzed by **2B** were also examined. When **2B** (0.05 mM in 2 mL DMF) was titrated by substrate flaH (4 mM, 0.2 eq. in 10 μL DMF) under N_2 at room temperature, an intense absorption band appeared at 402 nm (ESI, Fig. S9a). The value of λ_{max} is the same with the characteristic $\pi \rightarrow \pi^*$ transition of the coordinated substrate flavonolate of the ES model complex supported by the non-substituted analogue model ligand $[Fe^{III}L^H(fla)](OAc)$,[38] and matches well with those of the ES adducts of the native enzyme[14] and other synthetic metal flavonolate ES model complexes.[26,28,41,42] This feature in the optical spectrum, by analogy to these reported data, can be assigned to the $\pi \rightarrow \pi^*$ transition of the bound substrate flavonolate.[43] The absorbance at 402 nm increases linearly with the concentration of flaH, and attains a maximum value after addition of 2 eq. flaH ([flaH] = 0.1 mM, [**2B**] = 0.05 mM) and remains unaltered upon further addition of flaH (ESI, Fig. S9a, Insert), implying that the diiron(III) complex **2B** also could react with 2 eq. flaH to form 2 eq. mononuclear flavonolate complex $[Fe^{III}L(fla)]^+$, which could undergo dioxygenation reaction of the bound flavonolate described below. The formation of $[Fe^{III}L(fla)]^+$ was also confirmed by ESI-MS (m/z (pos.): 655.28 ($[Fe^{III}L(fla)]^+$)) (ESI, Fig. S9b). At the same conditions, the initial reaction rate of the dioxygenation of the substrate flavonol (1.0×10^{-4} M) catalyzed by **2B** (0.5×10^{-6} M) (4.30×10^{-10} M s^{-1} at 70 °C and 63.7×10^{-10} M s^{-1} at 100 °C) is much smaller (about 5 times) than that of $[Fe^{II}L(OAc)]$ (**2**) (1.0×10^{-6} M) (21.0×10^{-10} M s^{-1} at 70°C), and just between $[Zn^{II}L(OAc)]$ (**6**) (1.0×10^{-6} M) (144×10^{-10} M s^{-1} at 100 °C) and $[Mn^{II}L(OAc)]$ (**1**) (1.0×10^{-6} M) (58.0×10^{-10} M s^{-1} at 100 °C) in the catalytic dioxygenation reactivity order (ESI, Table S5). These results indicate that the reactivity order inconformity of $[Fe^{II}L(OAc)]$ (**2**) is really due to the formation of the less active diiron(III) μ-oxo complex **2B** during the catalytic reaction.

The reactivity of the dioxygenation of the substrate flavonol catalyzed by our model complexes $[M^{II}L(OAc)]$ was not influenced by the redox potential of the metal ion whether the metal ion is redox-active or redox-inert or non-redox metal ion. This results imply that the major role of the metal ion is to tune the redox potential of the bound substrate flavonolate and stabilize the flavonoxyl radical generated during the catalytic dioxygenation reaction by delocalization of the unpaired electron rather than to participate directly in redox chemistry (although the metal ion M^{II} was oxidized to M^{III} for the Fe^{II}- and Co^{II}-complexes and the Cu^{II} was reduced to Cu^{I} for the Cu^{II}-complex in the second step but it is not the rate-determining step of the reaction catalyzed by these complexes described below). Therefore, it can be concluded that the reactivity of the dioxygenation of the substrate flavonol catalyzed by our model complexes $[M^{II}L(OAc)]$ was strikingly influenced by the redox potential of the substrate flavonolate coordinated to the metal ion (the lower oxidation potential E_{pa}, the higher catalytic reactivity), which was affected by the metal ion of the model complexes via tuning the electron density of the bound substrate flavonolate through O(carbonyl)=C(4)−C(3)=C(2) "electron conduit", and the metal ion may be critical in controlling the enzymatic reactivity. All these emphasize the importance of the metal ion and provide important insights into the role of the metal ion.

Catalytic Mechanism. To determine the binding affinity of the substrate flavonol for $[M^{II}L(OAc)]$ in solution, optical spectral titrations were performed by gradual addition of flaH (3 mM, 0.1 eq. in 10 μL DMF) to a solution of $[M^{II}L(OAc)]$ (0.1 mM in 3 mL DMF) under N_2 at room temperature. An intense absorption band arose at 400 − 443 nm (Mn: 425 nm ($\varepsilon = 1.1 \times 10^4$ M^{-1} cm^{-1}), Fe: 400 nm ($\varepsilon = 9.6 \times 10^3$ M^{-1} cm^{-1}), Co: 422 nm ($\varepsilon = 9.8 \times 10^3$ M^{-1} cm^{-1}), Ni: 443 nm ($\varepsilon = 1.2 \times 10^4$ M^{-1} cm^{-1}), Cu: 424 nm ($\varepsilon = 1.1 \times 10^4$ M^{-1} cm^{-1}) and Zn: 421 nm ($\varepsilon = 1.8 \times 10^4$ M^{-1} cm^{-1})) (ESI, Fig. S9 and Fig. S10). The values of λ_{max} are the same with the characteristic $\pi \rightarrow \pi^*$ transition of the coordinated substrate flavonolate of the corresponding ES model complexes $[M^{II}L(fla)]$ [37,40] and similar to those of the non-substituted analogue ES model complexes $[M^{II}L^H(fla)]$,[38] and match well with those of the ES adducts of the native enzyme[14] and other synthetic metal flavonolate ES model comlexes.[26,28,41,42] These features in the optical spectra, by analogy with the reported data, can be assigned to the $\pi \rightarrow \pi^*$ transition of the coordinated substrate flavonolate.[43] The absorbance at the corresponding λ_{max} increases linearly with the concentration of flaH, and attains a maximum value after addition of 1 eq. flaH and remains unaltered upon further addition of flaH (ESI, Fig. S9), indicating that $[M^{II}L(OAc)]$ could react with 1 eq. substrate flaH to form the corresponding mononuclear metal-flavonolate complex $[M^{II}L(fla)]$ with displacement of co-ligand OAc^-. In such a case, the co-ligand OAc^- may act as a base to accept the proton of substrate flavonol flaH. The formation of $[M^{II}L(fla)]$ was also confirmed by ESI-MS, the peak cluster due to $[M^{II}L(fla)]H^+$ (M = Mn (**1**), Ni (**4**), Cu (**5**) and Zn (**6**)), $[Co^{II}L(fla)]Na^+$ for **3** and

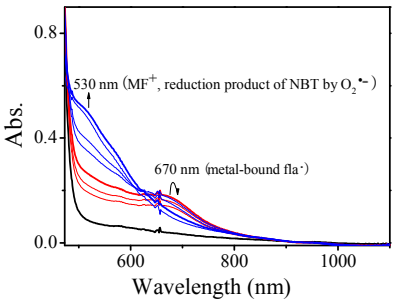

Fig. 6 Spectral changes for the reaction of flavonol (0.5 mM in DMF) (black line) with O_2 in the presence of equivalent amount of $[Mn^{II}L(OAc)]$ (red line) and excess NBT (blue line) at rt.

$[Fe^{III}L(fla)]^+$ for **2** (ESI, Fig. S10-Inset) was also observed. After the above solution of **3** was exposed to O_2, we observed a metal ion oxidized peak cluster at *m/z* (pos.) = 658.3 ($[Co^{III}L(fla)]^+$) (ESI, Fig. S10g). The *m/z* value and the isotope distribution pattern of each peak cluster are in good greement with the calculated values. All these results indicate that the substrate flavonol was coordinated to the M^{II} with displacement of the co-ligand OAc^- to form a mononuclear M^{II}-flavonolate complexes $[M^{II}L(fla)]$ at the first stage of the catalytic reaction. The Fe^{II}- and Co^{II}-flavonolate complexes are so sensitive to O_2 that the Fe^{II}/Co^{II} center was easily oxidized to Fe^{III}/Co^{III} prior to the dioxygenation of the bound flavonolate, while, no oxidation state change was observed in the ESI-MS spectrum for the Mn^{II}-, Ni^{II}-, Cu^{II}- and Zn^{II}-flavonolate complexes.

Interestingly, when the substrate flavonol react with O_2 in the presence of 1 eq. $[M^{II}L(OAc)]$, an absorption band arose at 670 nm (Fig. 6-red line for **1**), which is the same with the reported free flavonoxyl radical fla$^\bullet$ at 676 nm,[38,39] so it can be assigned to the flavonoxyl radical fla$^\bullet$ generated by one electron transfer from fla^- to O_2 with concomitant generation of free superoxide radical $O_2^{\bullet-}$. After the addition of excess nitrotetrazolium blue chloride (NBT^{2+}), a new absorption band arose at 530 nm (Fig. 6-blue line), indicating that NBT was reduced to monoformazan (MF^+) by the generated $O_2^{\bullet-}$.[44] At the same time, the band at 670 nm disappeared due to the instability of the bound fla$^\bullet$.

On the basis of the spectroscopic, redox property, kinetic and products analysis results, we propose the dioxygenation reaction mechanism of flavonol catalyzed by $[M^{II}L(OAc)]$ as follows.

Fe^{II}- and Co^{II}-complexes $[M^{II}L(OAc)]$ (M = Fe (**2**) and Co (**3**)) (Scheme 3): First, the substrate flavonol could coordinate to the M^{II} ion of catalyst $[M^{II}L(OAc)]$ with displacement of the co-ligand OAc^- to form the mononuclear M^{II}-flavonolate complex $[M^{II}L(fla)]$ (**A**), which may react with one O_2 molecule to generate $[M^{III}L(fla)]^+$ (**B**) and $O_2^{\bullet-}$ by one electron transfer from M^{II} to O_2 quickly. Then followed by the rate-determining direct one electron transfer from the bound fla^- to another O_2 molecule slowly to form flavonoxyl radical $[M^{III}L(fla^\bullet)]^{2+}$ (**C**) and $O_2^{\bullet-}$. After that, the generated $[M^{III}L(fla^\bullet)]^{2+}$ (**C**) and $O_2^{\bullet-}$ react quickly to form a dioxolane intermediate $[M^{III}L(fla\text{-}O_2)]^+$ (**D**). Then, there occur the O-O bond and two C-C bond cleavage resulting in the dioxygenation product complex $[M^{III}L(Obs)]^+$ (**E**) with concomitant release of CO. The final step of the mechanism between the Fe^{II}- and Co^{II}- complexes are different. For the Co^{II}-complex **3**, $[Co^{III}L(Obs)]^+$ (**E**) release the dioxygenation product HObs, and react with flaH to start the next catalytic cycle. While for the Fe^{II}-complex **2**, after $[Fe^{III}L(Obs)]^+$ (**E**) release HObs, the diiron(III) μ-oxo complex $[(Fe^{III}L)_2(\mu\text{-}O)(\mu\text{-}OAc)]^+$ (**2B**) was formed, which could react with 2 eq. flaH to start the next catalytic cycle.

Scheme 3. Proposed dioxygenation reaction mechanism of flavonol catalyzed by $[Fe^{II}/Co^{II}L(OAc)]$.

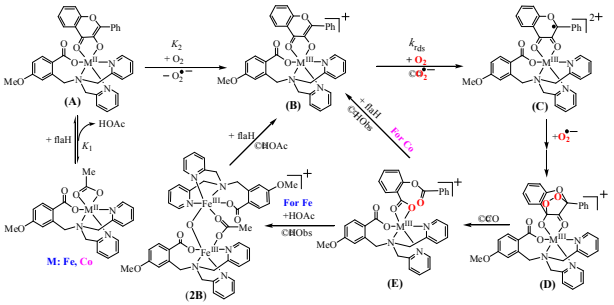

Mn^{II}-, Ni^{II}- and Zn^{II}-complexes $[M^{II}L(OAc)]$ (M = Mn (**1**), Ni (**4**) and Zn (**6**)) (Scheme 4-route a): The catalytic mechanisms of these complexes are similar to those of the Fe^{II}- and Co^{II}-complexes except the oxidation state change of the metal ion (second step from $[M^{II}L(fla)]$ to $[M^{III}L(fla)]^+$), and there also exist the rate-determining direct one electron transfer from the activated flavonol (fla^-) of $[M^{II}L(fla)]$ (**A**) to O_2 to generate $[M^{II}L(fla^\bullet)]^+$ (**C**) and $O_2^{\bullet-}$ slowly.

Scheme 4. Proposed dioxygenation reaction mechanism of flavonol catalyzed by $[Mn^{II}/Ni^{II}/Zn^{II}/Cu^{II}L(OAc)]$.

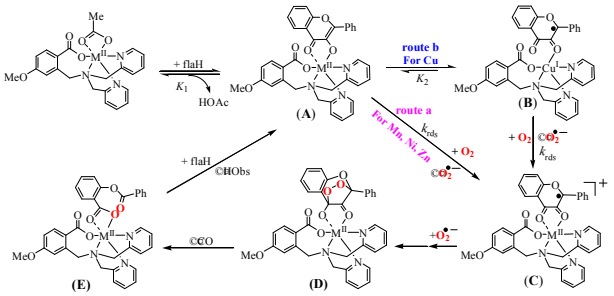

Cu^{II}-complex $[Cu^{II}L(OAc)]$ (**5**) (Scheme 4-route b): There is a fast equilibrium between the formed $[Cu^{II}L(fla)]$ (**A**) and $[Cu^{I}L(fla^\bullet)]$ (**B**). In which, the bound fla^- is activated by an intramolecular one electron transfer from fla^- to Cu^{II}, it is more favorable than dioxygen activation. Then the dioxygen is activated by Cu^I of $[Cu^{I}L(fla^\bullet)]$ (**B**) (one electron transfer from Cu^I to O_2) to form $[Cu^{II}L(fla^\bullet)]^+$ (**C**) and $O_2^{\bullet-}$ slowly, which is the rate-determining step. In such a case, the Cu(II) ion of the complex acts as an "electron buffer" for one electron transfer from the bound fla^- to O_2, activating the bound substrate flavonolate first, then dioxygen, successively.

Although the catalytic dioxygenation reaction mechanism of the complexes are not the same completely, they have the same rate-determining step, which is direct one electron transfer from the bound fla^- to O_2 molecule to form flavonoxyl radical fla$^\bullet$ and $O_2^{\bullet-}$. This results are consistent with the results that the reactivity of

the dioxygenation of the substrate flavonol catalyzed by our model complexes [$M^{II}L(OAc)$] was not affected by the redox potential of the metal ion whether the metal ion is redox-active or redox-inert or non-redox metal ion but drastically influenced by the redox potential of the substrate flavonolate bound to the metal ion, which was affected by the metal ion of the model complexes via tuning the electron density of the bound substrate flavonolate through the "electron conduit" O(carbonyl)=C(4)−C(3)=C(2).

The catalytic dioxygenation reaction mechanism of [$Cu^{II}L(OAc)$] is similar to that of the native Cu^{II}-containing 2,3-QD,[6,12,13] while the reaction mechanisms of [$M^{II}L(OAc)$] (M = Mn, Fe, Co, Ni and Zn) are similar to those of the Mn^{II}-, Fe^{II}-, Co^{II}-, Ni^{II}- and Zn^{II}-containing 2,3-QD, respectively.[9-11,14] They are very similar to the intra-diol and extra-diol catechol dioxygenase, respectively.[45]

Conclusion

In summary, in order to gain insights into the metal ion effects and the carboxylate effects on the enzymatic reactivity, a series of the carboxylate ligand supported complexes [$M^{II}L(OAc)$] (M = Mn (**1**), Fe (**2**), Co (**3**), Ni (**4**), Cu (**5**) and Zn (**6**)) have been synthesized and characterized as structural and functional models for the active site of various M^{II}-substituted resting 2,3-QD. Their structures, spectroscopic features, redox properties, as well as the catalytic reactivity toward substrate flavonol and O_2 have been investigated in detail. The complexes could effectively activate dioxygen to catalyze the oxygenative heterocyclic ring opening reaction of the substrate flavonol (enzymatic reaction). The catalytic reaction exhibits first-order dependence with respect to the model complex, the substrate flavonol and dioxygen, respectively. The model complexes show relatively high enzymatic reactivity on the catalytic dioxygenation of flavonol than other reported model complexes due to the carboxylate group of the supporting model ligand L^-, which could lower the redox potential of the bound substrate flavonolate by donating electron via the metal ion and O(carbonyl)=C(4)−C(3)=C(2) "electron conduit". The complexes exhibit strikingly different catalytic reactivity and it is in a metal ion dependent order of Co (**3**) > Ni (**4**) > Zn (**6**) > Fe (**2**) > Mn (**1**) > Cu (**5**). The differences on the reactivity among them may be contributed to the redox potential of the coordinated substrate flavonolate, which could be influenced by the metal ion of the model complexes [$M^{II}L(OAc)$] in different degrees, leading to different catalytic activity. The major role of the metal ion is to tune the redox potential of the bound substrate flavonolate via O(carbonyl)=C(4)−C(3)=C(2) "electron conduit" and stabilize the flavonoxyl radical generated during the dioxygenation reaction by delocalization of the unpaired electron rather than to participate directly in redox chemistry. It is significant that our model complexes [$M^{II}L(OAc)$] are the first example of a series of structural and functional models of various M^{II}-substituted resting 2,3-QD, providing important insights into the metal ion effects and the carboxylate effects of the model ligand on the enzymatic activity of various M^{II}-substituted 2,3-QD.

Experimental

General and physical methods

All reagents and solvents except the ligand LH were obtained from commercial sources and were used as received unless otherwise noted. Air-sensitive reactions were performed under N_2 atmosphere.

The crystal evaluations and intensity data were performed on a Bruker Smart APEXII CCD single-crystal diffractometer using Mo Kα radiation (λ = 0.71073 Å) at 296 K. Infrared spectra were recorded with a Nicolet 6700 instrument. UV–vis spectra were recorded on an Agilent 8453 diode-array spectrophotometer using quartz cells. ESI-MS and HPLC-MS spectrum were performed on a Thermo Fisher Scientific LTQ Orbitrap XL HPLC/ESI-MS with an on-line UV-vis detector (λ: 210 nm). EPR spectra of [$M^{II}L(OAc)$] (Mn (**1**), Fe (**2**), Co (**3**), Cu (**5**)) (4mM in 0.5 mL DMF) were obtained by using a Bruker A200 spectrometer at 100 K. The magnetic susceptibility was mesured using a Quantum Design SQUID (MPMS-XL-7) magnetometer at room temperature. Cyclic voltammetry data were collected using a CHI 610d system. All CV data were obtained under N_2 in DMF with $KClO_4$ (0.5 M) as the supporting electrolyte. The electrodes were as follows: glassy carbon (working), Pt sheet (auxiliary) and SCE (reference). ^1H NMR spectra were recorded on a Bruker 400WB. The production of the gas product CO during catalytic dioxygenation reaction was detected by online CO_x analyzer (SICK-MAIHAK-S710, Germany).

Synthesis of the model complexes

Model ligand **LH** was prepared according to the reported procedure.[37] The model complexes were synthesized according to the following procedure. A dry CH_3OH solution (3 mL) containing 0.1 mmol $M^{II}(OAc)_2{\cdot}nH_2O$ (n = 0 for Fe^{II} and 4 for others) was added dropwise to a CH_3OH (2 mL) solution of **LH** (36.3 mg, 0.1 mmol) at room temperature under N_2. After stirring for 30 min, the [$M^{II}L(OAc)$] was isolated as powder by treating with ether.

[$Mn^{II}L(OAc)$] (**1**). White powder, 43.8 mg, 92%. ESI-MS: *m*/*z* (pos.) = 417.2 ([$Mn^{II}L]^+$) (main peak), 477.03 ([$Mn^{II}L(OAc)]H^+$) (ESI, Fig. S1a). Colorless micro crystal was obtained by diffusion ether into the CH_2Cl_2 and CH_3OH solution. Anal Calc for $C_{23}H_{23}N_3MnO_5$ (476.38): C, 57.99; H, 4.87; N, 8.82. Found: C, 57.81; H, 5.03; N, 8.69. FT-IR (solid sample: KBr, cm^{-1}): 3252 (m), 1602 (s), 1557 (s), 1436 (m), 1413 (m), 1402 (m), 1372 (s), 1328 (w), 1242 (s), 1090 (s), 805 (s), 766 (s), 699 (m). FT-IR (solution sample: in ethanol, cm^{-1}): 3201 (m), 1602 (s), 1560 (s), 1445 (m), 1413 (s), 1370 (m), 1324 (m), 1236 (s), 1107 (m), 807 (m), 756 (s), 687 (s).

[$Fe^{II}L(OAc)$] (**2**). Yellowish-brown powder, 42.5 mg, 89%. ESI-MS: *m*/*z* (pos.) = 418.1 ([$Fe^{II}L]^+$), 450.1 ([$Fe^{II}L(CH_3OH)]^+$), 477.0 ([$Fe^{III}L(OAc)]^+$) (ESI, Fig. S1b). Anal. Calcd for $C_{23}H_{23}N_3FeO_5$ (477.29): C, 57.88; H, 4.86; N, 8.80. Found: C, 57.73; H, 4.99; N, 8.65. FT-IR (solid sample: KBr, cm^{-1}): 3382 (m), 1606 (s), 1557 (m), 1439 (m), 1402 (m), 1396 (m), 1372 (m), 1325 (m), 1248 (m), 1090 (s), 1045 (s), 1025 (s), 766 (s), 704 (m). FT-IR (solution sample: in ethanol, cm^{-1}): 3351 (m), 1594 (s), 1557 (m), 1440 (m), 1413 (m), 1394 (m), 1348 (m), 1324 (m), 1282 (m), 1258 (s), 1100 (s), 1024 (s), 794 (s), 765 (s). Brown single crystal [$(Fe^{II}LCl]_2{\cdot}4.5H_2O$ (**2A**) suitable for X-ray diffraction was obtained during the crystallization of [$Fe^{II}L(OAc)$] (**2**) in a glove box by diffusion ether into the CH_2Cl_2 and CH_3OH

solution. Since the mononuclear Fe^{II}-complex $[Fe^{II}L(OAc)]$ (**2**) is so air sensitive in solution, an auto-oxidized brown single crystal suitable for X-ray diffraction was also obtained by diffusion ether into the CH_2Cl_2 and CH_3OH solution under aerobic conditions with molecular formula $[(Fe^{III}L)_2(\mu\text{-}O)(\mu\text{-}OAc)]Cl\cdot 10H_2O$ (**2B**). In order to prove the reactivity inconformity of $[Fe^{II}L(OAc)]$ (**2**) maybe due to the formation of the less active **2B** during the catalytic reaction, **2B** was prepared independently under air and isolated as brown powder. ESI-MS: *m*/*z* (pos.) = 911.1 ($[(Fe^{III}L)_2(OAc)(O)]^+$). Anal. Calcd for $C_{44}H_{43.5}ClFe_2N_6O_{9.25}$ (951.49): C, 55.54; H, 4.61; N, 8.83. Found: C, 55.43; H, 4.75; N, 8.68. FT-IR (KBr, cm^{-1}): 3365 (m), 1592 (s), 1549 (w), 1526 (s), 1442 (m), 1381 (s), 1333 (m), 1259 (s), 1245 (s), 1095 (m), 1026 (m), 773 (s).

$[Co^{II}L(OAc)]$ (**3**). Pink powder, 39.4 mg, 82%. ESI-MS: *m*/*z* (pos.) = 421.0 ($[Co^{II}L]^+$) (main peak), 481.2 ($[Co^{II}L(OAc)]H^+$) (ESI, Fig. S1c). Anal. Calcd for $C_{23}H_{23}N_3CoO_5$ (480.38): C, 57.51; H, 4.83; N, 8.75. Found: C, 57.36; H, 4.98; N, 8.60. FT-IR (solid sample: KBr, cm^{-1}): 3420 (m), 1596 (m), 1570 (s), 1444 (m), 1420 (m), 1397 (s), 1256 (m), 1050 (m), 764 (m). FT-IR (solution sample: in ethanol, cm^{-1}): 3292 (m), 1600 (s), 1549 (s), 1405 (m), 1402 (m), 1383 (m), 1286 (m), 1247 (m), 1087 (s), 1046 (s), 762 (s). Purple single crystal $[Co^{II}LCl]_2\cdot 4H_2O$ (**3A**) suitable for X-ray diffraction was obtained during the crystallization of $[Co^{II}L(OAc)]$ (**3**) by diffusion ether into the CH_2Cl_2 and CH_3OH solution.

$[Ni^{II}L(OAc)]$ (**4**). Greenish powder, 43.1 mg, 90%. ESI-MS: *m*/*z* (pos.) = 420.2 ($[Ni^{II}L]^+$), 480.2 ($[Ni^{II}L(OAc)]H^+$) (main peak) (ESI, Fig. S1d). Anal. Calcd for $C_{23}H_{23}N_3NiO_5$ (480.14): C, 57.53; H, 4.83; N, 8.75. Found: C, 57.37; H, 4.97; N, 8.58. FT-IR (solid sample: KBr, cm^{-1}): 3324 (m), 1605 (s), 1550 (s), 1444 (m), 1417 (s), 1392 (s), 1101 (s), 1048 (s), 766 (s). FT-IR (solution sample: in ethanol, cm^{-1}): 3291 (m), 1605 (s), 1558 (s), 1443 (m), 1417 (s), 1402 (m), 1364 (s), 1102 (s), 1023 (m), 766 (m). Light-blue single crystal $[Ni^{II}L(CH_3OH)]_2Cl_2\cdot 3.5H_2O$ (**4A**) suitable for X-ray diffraction was obtained during the crystallization of $[Ni^{II}L(OAc)]$ (**4**) by diffusion ether into the CH_2Cl_2 and CH_3OH solution.

$[Cu^{II}L(OAc)]\cdot 0.5CH_3OH\cdot 1.5H_2O$ (**5**). Blue powder, 36.3 mg, 75%. ESI-MS: *m*/*z* (pos.) = 425.0 ($[Cu^{II}L]^+$)(main peak), 461.0 ($[Cu^{II}L(H_2O)_2]^+$), 485.0 ($[Cu^{II}L(OAc)]H^+$) (ESI, Fig. S1e). Anal. Calcd for $C_{23.5}H_{28}CuN_3O_7$ (528.04): C, 53.45; H, 5.34; N, 7.96. Found: C, 53.36; H, 5.51; N, 7.83. FT-IR (solid sample: KBr, cm^{-1}): 3323 (m), 1610 (s), 1574 (s), 1410 (s), 1381 (m), 1349 (s), 1088 (s), 1047 (s), 879 (s), 761 (m). FT-IR (solution sample: in ethanol, cm^{-1}): 3284 (m), 1609 (s), 1576 (s), 1409 (s), 1379 (s), 1351 (s), 1120 (m), 764 (m). Blue single crystal suitable for X-ray diffraction was obtained by diffusion ether into the CH_2Cl_2 and CH_3OH solution with molecular formula $[Cu^{II}L(OAc)]\cdot 0.5CH_3OH\cdot 1.5H_2O$ (**5**).

$[Zn^{II}L(OAc)]$ (**6**). Yellow powder, 44.3 mg, 91%. ESI-MS: *m*/*z* (pos.) = 426.2 ($[Zn^{II}L]^+$) (main peak), 486.3 ($[Zn^{II}L(OAc)]H^+$), 508.3 ($[Zn^{II}L(OAc)]Na^+$), (ESI, Fig. S1f). Anal. Calcd for $C_{23}H_{23}ZnN_3O_5$ (486.84): C, 56.74; H, 4.76; N, 8.63. Found: C, 56.56; H, 5.01; N, 8.46. FT-IR (solid sample: KBr, cm^{-1}): 3401 (m), 1604 (s), 1583 (s), 1483 (m), 1439 (s), 1390 (s), 1285 (m), 1255 (m), 765 (m). FT-IR (solution sample: in ethanol, cm^{-1}): 3401 (m), 1605 (s), 1583 (s), 1483 (m), 1440 (s), 1391 (s), 1285 (m), 1255 (m), 1022 (m), 765 (m).

Kinetic measurements

[flaH] or $[M^{II}L(OAc)]$-dependence and determination of the activation parameters

The reactions of substrate flavonol with O_2 catalyzed by the complexes $[M^{II}L(OAc)]$ were performed in a 10 mm path length UV-vis cell that was held in a Unisoku thermostatted cell holder USP-203 (a desired temperature can be fixed within ± 0.5 °C). After the solution of substrate flavonol ($0.79 - 1.3 \times 10^{-4}$ M in 2.95 mL DMF) was kept at a desired temperature (55 − 100 °C) under N_2 for several minutes, the catalyst complexes $[M^{II}L(OAc)]$ ($0.50 - 5.0 \times 10^{-6}$ M in 50 μL DMF, 0.5 − 5.0%) were injected and the N_2 was replaced with O_2. The time courses of the reactions were followed by monitoring the absorption changes of the substrate flavonol at 343 nm (log ε = 4.24). The activation parameters for the catalytic dioxygenation reactions were obtained from an Eyring plot and an Arrhenius plot (Table 4, ESI, Table S5 and Fig. S4) at the temperature range of 55 − 100 °C.

$[O_2]$-dependence

In a typical experiment, deaerated 58 mL DMF solution of substrate flavonol (~1.0×10^{-4} M) in a thermostatted reaction vessel (connecting to a manometer to regulate constant dioxygen pressure) was kept at a desired temperature (55 − 100 °C) under N_2 for several minutes. The deaerated DMF solution of $[M^{II}L(OAc)]$ ($1.0 - 5.0 \times 10^{-6}$ M) were added to above solution. Then the N_2 was replaced with a desired constant pressure dioxygen through a manometer to start the reaction. The reaction mixture was then taken by syringe periodically (ca. every 3 − 5 min), and the time course of the reaction was followed by monitoring the absorption changes at 343 nm (log ε = 4.24). The O_2 concentrations in DMF were calculated from literature data taking into account the partial pressure of DMF[46] and assuming the validity of Dalton's law.[47]

Reaction product analysis

By HPLC-MS

The substrate flavonol (6.0 mg, 0.025 mmol) and catalyst model complexes $[M^{II}L(OAc)]$ (~0.60 mg, 0.00125 mmol) were dissolved in 5 mL DMF and stirred at 70/100 °C under dioxygen atmosphere for 12 hrs. After the reaction, the mixture was concentrated by evaporator, and the remaining residue was dissolved in 1.9 mL CH_3OH. *o*-Methylbenzoic acid (10 mM in 100 μL CH_3OH, total 0.5 mM in 2.0 mL solution) was added to the above solution as an internal standard. A Hypersil GOLD C18 column (Thermo Fisher Scientific 150 mm × 4.6 mm, 5 μm) was used for the HPLC analysis at room temperature with a mobile phase CH_3OH and 5 mM NH_4OAc solution with some gradient at a constant flow rate of 0.5 mL min^{-1}. The yields of the products were calculated using the standard calibration curve.

By ^1H NMR

The dioxygenation of flavonol (2.5×10^{-2} M in 200 mL DMF) catalyzed by $[Co^{II}L(OAc)]$ (**3**) (5% mol) was examined under O_2 at 100 °C for 7 days. The reaction mixture was esterificated by CH_3OH in the presence of H_2SO_4 after solvent evaporation, then extracted with CH_2Cl_2. The products were separated by using silica gel column chromatography. Two main reaction products salicylic acid and benzoic acid methyl esters were isolated successfully and identified by ^1H NMR (in $CDCl_3$).

CO Analysis

A home made reactor was linked with a pure N_2, an O_2 gas tank and an online CO_x analyzer. Dry N_2 gas (100 mL min^{-1}) was continuously supplied by bubbling to a deaerated DMF solution (10 mL) of flavonol (3.0×10^{-3} M) in the reactor for 30 min to degas the CO, CO_2 and O_2 in solution, reactor and all of the system lines. The solution was kept at 70 °C for several minutes until the CO concentrations were lower than 3 ppm. Then the solution of [Co^{II}L(OAc)] (**3**) (30 mM in 50 µL DMF, 5% mol ratio) was injected and dry O_2 and N_2 gas (30:70) were continuously supplied by bubbling (100 mL min^{-1}) and the analysis were started and the online CO gas concentrations were recorded for 104 min. After about 50 min, the CO concentration was lower than 6 ppm and did not change for about 50 min, we stopped the detection of CO. The total CO concentration was integrated for the whole reaction time.

Acknowledgments

The authors are grateful for the financial support of the National Natural Science Foundation of China (No. 21471025).

Notes and references

1 E. Wollenweber, in: J. B. Harborne, T.J. Mabry (Eds.), Flavonoids: Advances in Research, Chapman & Hall, London, New York, 1982, p. 189.

2 W. Bors, W. Hellers, C. Michel, *Meth. Enzymol.*, 1990, **186**, 343–354.

3 Y. Hanasaki, S. Ogawa, S. Fukui, *J. Free Radic. Biol. Med.*, 1992, **16**, 605–608.

4 J. P. Hu, M. Calomme, A. Lasure, T. De Bryune, L. Pieters, A. Vlietnick, D. D. A. Vanden Berghe, *Biol. Trace Elem. Res.*, 1995, **47**, 327–331.

5 C. A. Rice-Evans, N. J. Miller, G. Pananga, *J. Free Radic. Biol. Med.*, 1996, **20**, 933–956.

6 F. Fusetti, K. H. Schröter, R. A. Steiner, P. I. van Noort, T. Pijning, H. J. Rozeboom, K. H. Kalk, M. R. Egmond, B. W. Dijkstra, *Structure*, 2002, **10**, 259–268.

7 T. Oka, F. J. Simpson, *Biochem. Biophys. Res. Commun.*, 1971, **43**, 1–5.

8 H.-K. Hund, J. Breuer, F. Lingens, J. Hüttermann, R. Kappl, S. Fetzner, *Eur. J. Biochem.*, 1999, **263**, 871–878.

9 Gopal, B.; Madan, L. L.; Betz, S. F.; Kossiakoff, A. A. *Biochemistry*, 2005, **44**, 193–201.

10 B. M. Barney, M. R. Schaab, R. LoBrutto, W. A. Francisco, *Protein Expr. Purif.*, 2004, **35**, 131–141.

11 L. Bowater, S. A. Fairhurst, V. J. Just, S. Bornemann, *FEBS Lett.*, 2004, **557**, 45–48.

12 R A. Steiner, K. H. Kalk, B. W. Dijkstra, *Proc. Natl. Acad. Sci.*, 2002, **99**, 16625–16630.

13 R. A. Steiner, I. M. Kooter, B. W. Dijkstra, *Biochemistry*, 2002, **41**, 7955–7962.

14 (a) M. R. Schaab, B. M. Barney, W. A. Francisco, *Biochemistry*, 2006, **45**, 1009–1016. (b) H. Merkens, R. Kappl, R. P. Jakob, F. X. Schmid, S. Fetzner, *Biochemistry*, 2008, **47**, 12185–12196. (c) D. Nianios, S. Thierbach, L. Steimer, P. Lulchev, D. Klostermeier, S. Fetzner, *BMC Biochemistry*, 2015, **16**, 1–11.

15 (a) Dai, Y.; Pochapsky, T. C.; Abeles, R. H. *Biochemistry,* 2001, **40**, 6379–6387. (b) Fielding, A. J.; Kovaleva, E. G.; Farquhar, E. R.; Lipscomb, J. D.; Que Jr, L. J. *Biol. Inorg. Chem.,* 2011, **16**, 341–355.

16 (a) Kaizer, J.; Balogh-Hergovich, E.; Czaun, M.; Casy, T.; Speier, G. *Coord. Chem. Rev.* **2006**, *222*, 2222–2233. (b) Pap, J. S.; Kaizer, J.; Speier, G. *Coord. Chem. Rev.* **2010**, *254*, 781–793. (c) Kaizer, J.; Pap, J. S; Speier, G. *Copper Dioxygenases. in Copper-Oxygen Chemistry*; Karlin, K.D., Shinobu, I. Eds.; John Wiley & Sons, Inc., Hoboken, New Jersey, 2011, pp 23–52.

17 (a) J. Kaizer, S. Góger, G. Speier, M. Réglier, M. Giorgi, *Inorg. Chem. Commun.*, 2006, **9**, 251–254. (b) É. Balogh-Hergovich, J. Kaizer, J. Pap, G. Speier, G. Huttner, L. Zsolnai, *Eur. J. Inorg. Chem.*, 2002, **9**, 2287–2295.

18 L. Barhács, J. Kaizer, J. Pap, G. Speier, *Inorg. Chim. Acta*, 2001, **320**, 83–91.

19 É. Balogh-Hergovich, J. Kaizer, G. Speier, *Inorg. Chim. Acta*, 1997, **256**, 9–14.

20 É. Balogh-Hergovich, J. Kaizer, G. Speier, *J. Mol. Catal. A: Chem.*, 2000, **159**, 215–224.

21 A. Y. S. Malkhasian, M. E. Finch, B. Nikolovski, A. Menon, B. E. Kucera, F. A. Chavez, *Inorg. Chem.*, 2007, **46**, 2950–2952.

22 J. Volkman, K. M. Nicholas, *Tetrahedron*, 2012, **68**, 3368–3376.

23 A. Nishinaga, T. Tojo, T. Matsuura, J. Chem. Soc., *Chem. Commun.*, 1974, **21**, 896–897.

24 J. S. Pap, A. Matuz, G. Baráth, B. Kripli, M. Giorgi, G. Speier, J. Kaizer, *J. Inorg. Biochem.*, 2012, **108**, 15–21.

25 É. Balogh-Hergovich, J. Kaizer, G. Speier, *J. Mol. Catal. A: Chem.*, 2003, **206**, 83–87.

26 G. Baráth, J. Kaizer, G. Speier, L. Párkányi, E. Kuzmann, A. Vértes, *Chem. Commun.*, 2009, 3630–3632.

27 P. Brydon, *Ph. Magaz. Lett.*, 1999, **79**, 383–387.

28 K. Grubel, K. Rudzka, A. M. Arif, K. L. Klotz, J. A. Halfen, L. M. Berreau, *Inorg. Chem.*, 2010, **49**, 82–96.

29 G. B. Deacon, R. J. Phillips, *Coord. Chem. Rev.*, 1980, **33**, 227–250.

30 G. Christou, S. P. Perlepes, E. Libby, K. Folting, J. C. Huffman, R. J. Webb, D. N. Hendrickson, *Inorg. Chem.*, 1990, **29**, 3657–3666.

31 A. B. P. Lever, Inorgnic Electronic Spectroscopy, 2nd edn. Elsevier, Amsterdam, 1984.

32 G. H. Reed, G. D. Markham, Biological Magnetic Resonance, L. J. Berliner, J. Rueben (Eds.), Plenum: New York, 1978, p. 73–142.

33 B. J. Hathaway, A. A. G. Tomlinson, *Coord. Chem. Rev.*, 1970, **5**, 1–43.

34 B. J. Hathaway, D. E. Billing, *Coord. Chem. Rev.*, 1970, **5**, 143–207.

35 H. Yokoi, *Bull. Chem. Soc. Jpn.*, 1974, **47**, 3037–3040.

36 I. M. Kooter, R. A. Steiner, B. W. Dijkstra, P. I. van Noort, M. R. Egmond, M. Huber, *Eur. J. Biochem.* 2002, **269**, 2971–2979.

37 Y. -J. Sun, Q. -Q. Huang, J. -J. Zhang, *Inorg. Chem.*, 2014, **53**, 2932–2942.

38 Y. -J. Sun, Q. -Q. Huang, T. Tano, S. Itoh, *Inorg. Chem.*, 2013, **52**, 10936–10948.

39 L. Barhács, J. Kaizer, G. Speier, *J. Org. Chem.*, 2000, **65**, 3449–3452.

40 Y. -J. Sun, Q. -Q. Huang, J. -J. Zhang, *Dalton Transactions*, 2014, **53**, 6480–6489.

41 R. F. V. De Souza, E. M. Sussuchi, W. F. De Giovani, *Synth. and React. in Inorg. and Met.-Org. Chem.*, 2003, **33**, 1125–1144.

42 A. Matuz, M. Giorgi, G. Speier, J. Kaizer, *Polyhedron*, 2013, **63**, 41–49.

43 L. Jurd, T. A. Geissman, *J. Org. Chem.*, 1956, **21**, 1395–1401.

44 B. H. J. Bielski, G. G. Shiue, S. Bajuk, *J. Phys. Chem.*, 1980, **84**, 830–833.

45 T. D. H. Bugg, G. Lin, *Chem. Commun.*, 2001, 941−952.

46 A. Kruis, Landolt-Börnstein, Board 4, Teil 4, Springer-Verlag, Berlin, 1976, p. 269.

47 G. Ram and A. R. Sharaf, *J. Ind. Chem. Soc.*, 1968, **45**, 13–16.

A series of the complexes [$M^{II}L(OAc)$] (M: Mn, Fe, Co, Ni, Cu and Zn) are reported as the first example of structural and functional models of various M^{II}-substituted quercetin 2,3-dioxygenase (M^{II}-2,3-QD), which exhibit strikingly different high enzymatic reactivity due to the existing carboxylate group in the ligand, providing important insights into the effects of the metal ion and carboxylate on the enzymatic activity of M^{II}-2,3-QD.